J. Fluid Mech. (2000), *vol.* 419, *pp.* 125–149. Printed in the United Kingdom

On the tip-splitting instability of viscous fingers

By E. LAJEUNESSE AND Y. COUDER

Laboratoire de Physique Statistique, Ecole Normale Supérieure 24 rue Lhomond, 75231 Paris Cedex 05, France

(Received 26 July 1999 and in revised form 16 December 1999)

The instabilities of Saffman–Taylor viscous fingers are revisited experimentally in the standard linear channel as well as in wedges of angle θ_0. The local destabilization of a finger occurs by a splitting of its tip and results in the formation of two branches separated by a fjord. It is shown that, in a first approximation, the central line of a fjord follows a curve normal to the successive profiles of stable fingers. These normal curves are computed analytically for the Saffman–Taylor finger in a linear cell and numerically for the wedges. The length of a fjord is critically sensitive to the position of the initial destabilization of the finger. The nearer to the tip it occurs, the longer the fjord will be. Assuming a uniform spatial distribution of the disturbances in the central part of the finger front it is possible to predict the size distribution of the lateral branches. In the linear channel the probability of branches larger than the channel width is negligible. For wedges of increasing angle the probability of large secondary branches increases. Finally, for wedges with θ_0 larger than approximately 90° infinite fjords separating two long-lived structures are observed. Our experimental results also suggest a generalization of the definition of virtual cells. With this new definition it is possible to show that the increasing complexity of the patterns corresponds to a hierarchy of virtual cells of various sizes.

1. Introduction

Saffman–Taylor fingering has become an archetype for systems in which growth occurs in a Laplacian field. As initially demonstrated by Paterson (1984) it is, in that respect, similar to the growth of aggregates produced by the model of diffusion-limited aggregation (DLA) due to Witten & Sander (1981, 1983). In both systems there is spontaneous formation of a ramified pattern which grows, essentially, at the protruding extremities. Rauseo, Barnes & Maher (1987), Couder (1988), and May & Maher (1989) checked experimentally that the fractal properties of large Saffman–Taylor patterns are similar to those of DLA aggregates. One of the basic questions about the fractal regime of growth is that structures of all sizes are constantly generated by the instability. How does this occur in viscous fingering? This will be the central question we will be concerned with in this article.

We shall now present the Saffman–Taylor problem and a few of the main classical results. This instability occurs in a Hele-Shaw cell when a very viscous fluid (e.g. oil) is displaced by a fluid of low viscosity (e.g. air). In this situation, a plane interface between the two fluids is unstable on a scale given by

$$l_c = \pi b \sqrt{\frac{\gamma}{\mu V}}, \tag{1}$$

where μ is the viscosity of the oil, γ the interfacial tension, b the thickness of the cell

and V the velocity of the front. This scale is obtained as the most unstable wavelength given by the linear stability analysis of Chuoke, Van Meurs & Van der Pol (1959) for the initial destabilization of a plane front.

For our present purpose an interesting feature of viscous fingering is that a whole range of behaviour can be observed which depends on the confinement of the system. Here we will investigate patterns grown in well-known confined geometries. These are the linear channel due to Saffman & Taylor (1958) and the sector-shaped cells introduced by Thomé *et al.* (1989). In both geometries two types of structures are known:

(i) When the effect of the confinement is important (l_c of the order of the cell width), stable fingers propagate in these channels. These solutions are now well documented. The analytical expressions for both their shape and their selection process are known.

(ii) When the confinement is weak (l_c small compared to the cell size), the curved fronts are not stable and for very weak confinements the structure observed becomes fractal.

In linear channels the usual control parameter is B given by

$$B = \frac{\gamma}{12\mu V}\left(\frac{b}{W}\right)^2 = 8.45 \times 10^{-3}\left(\frac{l_c}{W}\right)^2, \tag{2}$$

where V is the velocity of the Saffman–Taylor finger. B is thus proportional to the square of the ratio of the capillary length l_c in the tip region to the width of the channel W. This parameter is a measure of the confinement, which is reduced when B decreases. For moderate values of B a stable curved front, the classical Saffman–Taylor finger, is observed to propagate steadily in the cell. As B decreases it tends to occupy a fraction $\lambda = 0.5$ of the channel's width. Neglecting surface tension, Saffman & Taylor found a family of possible analytical shapes for the interface, parameterized by their width λ. The selection of the actual finger was solved in numerical investigations by McLean & Saffman (1981) and Vanden-Broeck (1983) and understood analytically by Combescot *et al.* (1986, 1988), Hong & Langer (1986), and Shraiman (1986). In these works, it was shown that taking surface tension into account there is, at a given B, selection of a discrete set of solutions labelled $n = 0$, $n = 1$, $n = 3\ldots$. The width λ of all these solutions tends to 0.5 when B tends to zero. The solution $n = 0$ of smallest λ at a given B was shown (by Bensimon, Pelcé & Shraiman 1987; Tanveer 1987; and Kessler, Koplik & Levine 1988) to be linearly stable down to $B = 0$. However, experimentally, the finger is unstable at small B as shown by Tabeling, Zocchi & Libchaber (1987) and Kopf-Sill & Homsy (1988).

This selection of the solution $\lambda = 0.5$ by surface tension acting at the tip is strongly supported by experiments. For instance it has been shown (Rabaud, Couder & Gerard 1988) that a local disturbance at the tip is sufficient to change the selection mode and to give rise to anomalous narrow fingers. Similarly, the experiments described below which are done in sector-shaped cells (Thomé *et al.* 1989) show a shift of the selected λ. This effect has been quantitatively interpreted as due to the effect of surface tension (Ben Amar *et al.* 1991). For this reason recent results due to Mineev-Weinstein (1998) and Aldushin & Matkowitch (1999) are surprising. These authors provide criteria that single out a steadily propagating finger of width $\lambda = 0.5$ from the continuum of steady finger solutions found by Saffman & Taylor. The relation between these new results and the classical ones on the effect of surface tension is not yet clear and remains a subject of debate.

In a sector-shaped cell, the viscous finger moves between two lateral walls forming an angle θ_0. We are mainly interested here in the cases where the front moves in a divergent direction ($\theta_0 > 0$). Thomé *et al.* (1989) observed experimentally that viscous fingering in a wedge gives rise to self-similar fingers which undergo a selection process analogous with that observed in the linear geometry. The parameter controlling the growth can be defined, by analogy with the linear channel, as $B = 8.45 \times 10^{-3}(l_c/\theta_0 r_T)^2$ where r_T is the distance from the tip to the apex and $W_T(r) = \theta_0 r_T$ is the channel width in the region of the tip. The finger width is defined as $\lambda = \theta_b/\theta_0$, θ_b being the angular width of the finger. For each angle, in the absence of surface tension, a family of self-similar analytical fingers is found (Ben Amar 1991) again parameterized by λ. The selection of the solution in the presence of isotropic surface tension has been investigated both numerically and analytically (Ben Amar *et al.* 1991 and Combescot & Ben Amar 1991). As in the linear cell, there is selection of a discrete set of solutions and the observed finger corresponds to the solution of smallest λ. Compared to the set selected for $\theta_0 = 0$, these solutions have widths λ shifted to larger values. The larger the angle the larger the shift. A remarkable feature is that these solutions do not exist for all B values: at a finite value $B_{th}(\theta_0)$, the levels $n = 0$ and $n = 1$ merge, so that there are no stable solutions for $B < B_{th}(\theta_0)$.

Traditionally, two terms are used in the literature to describe the destabilization of viscous fingers: tip splitting and side branching. In fact, in all isotropic Saffman–Taylor fingers the destabilization occurs in the front part of the finger so that here we will always call it tip splitting; the term 'side branching' should be reserved for the lateral destabilization which is a characteristic of anisotropic growth (dendritic crystal or anomalous Saffman–Taylor fingering, see Couder 1991). For these specific patterns the front part of the structure is parabolic, scaled on l_c and stable at all velocities. The instability grows progressively (see e.g. Rabaud *et al.* 1988) along the sides of the finger and becomes visible only far downstream of the tip.

In the limit of very weak confinement (very small values of B), the two length scales l_c and W are very far apart and a complex structure is observed which is fractal for the scales between l_c and W (Arnéodo *et al.* 1989). It was shown in that work that if ensemble averages were performed on many fractal patterns obtained in the same channel, the region having a large mean occupancy had the shape and width of the Saffman–Taylor stable solution. This property is valid for both Saffman–Taylor fingering and DLA. It is strictly true for the growth in a linear channel. In the wedges the width of the stable finger is recovered but not the shape; the ensemble average shows a tendency to split (Levine & Tu 1992; Arnéodo *et al.* 1996). In the case of DLA Brenner, Levine & Tu (1991) proposed a modified version of the mean field equations where most of these results are recovered.

Finally, the most widely investigated geometry for fractal growth is the axisymmetric configuration. Patterns of this type can be obtained from the Saffman–Taylor instability when the viscous fingers grow in the radial geometry introduced by Bataille (1968) and Paterson (1981). In this case the initial growth around the injection hole is circular until the front becomes deformed and a few indentations (usually five of them) form. Though the position of these indentations is not predetermined, they are correlated as they are separated by a distance of the order of l_c. At these points, which we will call 'stop points', the front curvature is reversed and the growth stops. After this initial destabilization the front forms fingers, each of them growing radially between two stop points and separated from its neighbours by 'fjords' (zones inside which the oil remains motionless). It was shown by Thomé *et al.* (1989) that these fingers grow as if enclosed between virtual walls defining wedge-shaped cells. As they

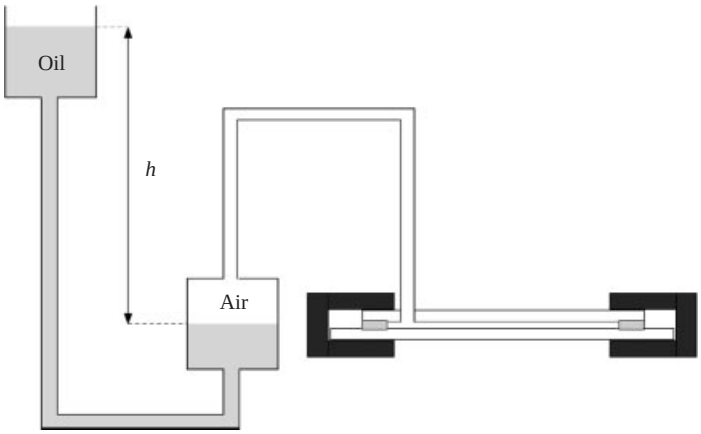

FIGURE 1. Schematic of the experimental set-up.

continue growing, the fingers in each of these virtual cells destabilize and tend to form complex 'trees'. However, even when the growth has formed a fractal object, the initial breaking of the symmetry appears to persist and to be at the origin of the formation of large independent trees.

The article is organized as follows. After describing (in § 2) the experimental set-up, we present the various results in the following sections. Section 3 is devoted to the measurement of the instability thresholds and their comparison to theory. In § 4 it is shown that the shape of the fjords separating the branches can be predicted from the initial position of the disturbance. Furthermore, these fjords can be used to define virtual cells and to predict the shape and stability of the branches. In § 5, using the distribution of the possible disturbances of the finger, we predict the fjord length distribution. Finally, in § 6, we make an attempt to generalize the concept of virtual cells to the description of complex patterns and to see how deterministic the pattern can be. Section 7 is the conclusion.

2. Experimental set-up

The instability of viscous fingers was investigated in a linear cell, in seven different wedges and in the circular geometry. All the wedge-shaped cells were made using only three pairs of glass plates. All the plates had a thickness of 1.2 cm, large enough to avoid flexion at the pressures we used. The first pair of plates was wedge shaped with angles $\theta_0 < 80°$. They were clamped together, separated from each other by sheets of Mylar of thickness 0.35 and 0.48 mm. These Mylar sheets served as spacers to fix the thickness of the cell. They also formed the lateral walls and were cut so as to impose the chosen geometry. The lateral walls were all designed in order that the resulting shape of the cell be a sector of a circle of angle θ_0 and of radius 57 cm, the air being injected exactly at the centre of the circle. The second pair of plates was used to obtain cells of larger angles (up to 180°). These had a smaller radius of 24 cm. Finally the last pair of glass plates, circular and of radius 24 cm, was used for radial fingering experiments.

Our experiments all used air to force oil out of the cell. We used four kinds of Rhodorsil Silicon oils: R47V10, R47V20, R47V100 and R47V500, having dynamical viscosity respectively 8.7, 19.9, 106.4 and 496 cP. Air was injected at the centre of the sector with a constant pressure defined by the hydrostatic pressure imposed by two

communicating vessels (figure 1). The first vessel, filled with oil in contact with the atmospheric pressure P_0, was connected to a second vessel partially filled with the air to be injected in the cell. The air pressure was therefore controlled by the difference h between the two levels of oil. The diameter of the vessels was large enough so that the variation of h was very small for the duration of an experiment.

With a constant-pressure injection, the interface local velocity has to be deduced from Darcy's law and is therefore non-trivially related to the distance r from the cell's centre. The finger is observed to slow down slightly at the beginning of its growth and to accelerate when it approaches the extremity of the cell. But in most of the cell the finger velocity can be, to a good approximation, taken as constant. This implies that in a wedge the parameter B decreases constantly during the growth.

Images of the pattern growth, recorded on video tapes by means of a CCD camera, were digitized using a Scion frame grabber connected to a computer and allowing us to acquire up to 25 images per second. We used the digitized images to measure the finger velocity and width and to analyse the finger shapes. From the velocity and width, we deduced B and λ. The digitized images were also used to compare the shape of the lateral branches to those predicted by the model (to be developed in § 4).

3. Threshold of destabilization of fingers

3.1. *Measurement of the threshold of destabilization of fingers*

Figures 2 and 3 show the typical evolution of a Saffman–Taylor finger in the case of a small and a large angle respectively. At the initial stages of the growth, stable curved fronts are observed, characterized by a monotonic curvature along the whole front (figure 2*a*). If the parameter B is kept constant (corresponding to a velocity decreasing as r^{-2}), a strict self-similar growth would be observed. In our experiments however, the front velocity is constant so that B decreases constantly because of the increase of the local width. The experimental results of Thomé *et al.* (1989) suggest that the finger adapts 'adiabatically' to the evolution of the local parameter B defined in the tip region.

As a result of the decrease of B the finger is observed to destabilize as shown on figures 2(*b*) and 3(*a*). This occurs presumably when B reaches the value at which the theory predicts that the level $n = 0$ vanishes (figure 4) (Ben Amar *et al.* 1991).

To test this hypothesis, we first checked that the relative finger width $\lambda(\theta_0)$ at destabilization coincides with the limit width of the level $n = 0$. As already observed by Ben Amar *et al.* (1991) the results, given on figure 5(*a*), are in good agreement with the theoretical predictions.

We then measured the local value B_{ex} at which this instability occurs. The exact location of the finger destabilization being difficult to determine exactly, we chose to measure B_{ex} at the radial position where one can distinguish a flattening at the finger tip. For each angular sector, we performed between 20 and 40 measurements of B_{ex}, varying the injection pressure and therefore the interface velocity (which is measured using digitized images). The value of B_{ex} and the error bar were estimated from this set of measurements. The measured values of B_{ex} are compared to the theoretical predictions B_{th} of Ben Amar *et al.* (1991) as a function of the cell angle θ_0 on figure 5(*b*).

3.2. *On the non-dimensional width of the finger at the destabilization*

These results can be presented in a different way. The parameter B, although useful, does not give an intuitive feeling for the experimental situation of the finger front for at least two reasons. First, it compares the square of a length scale characterizing the

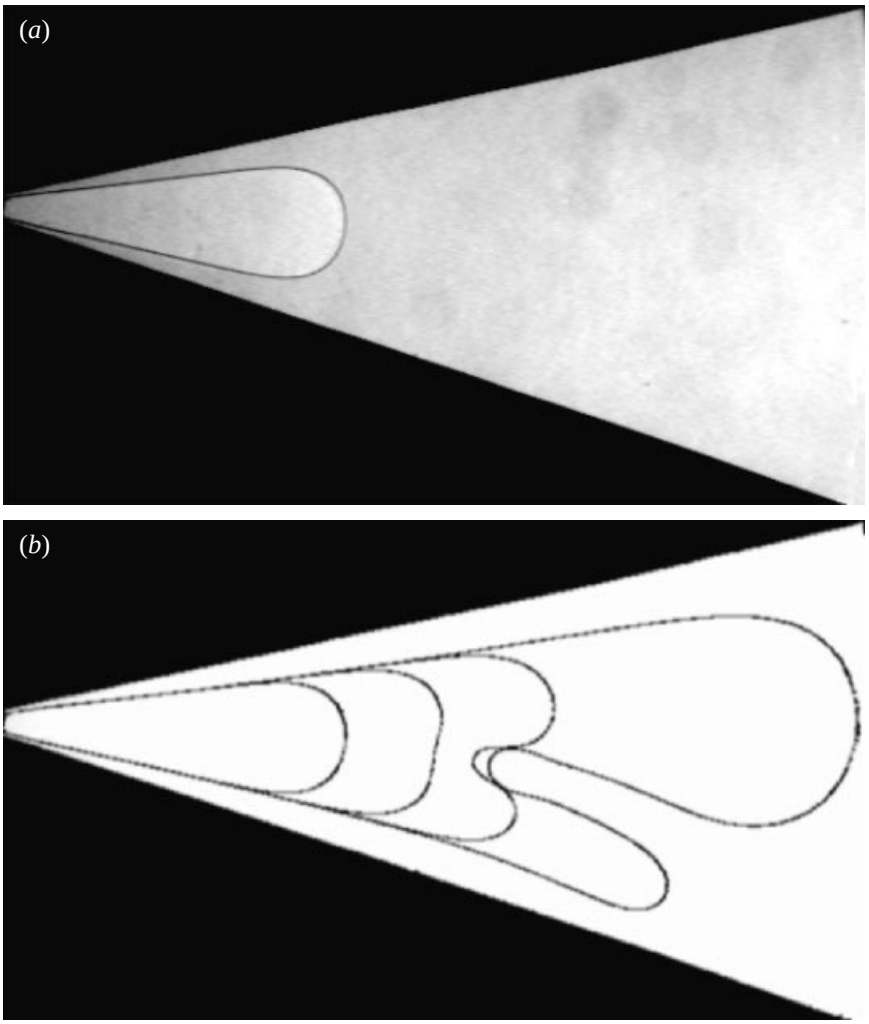

FIGURE 2. (*a*) A stable Saffman–Taylor finger in a sector-shaped cell of angle $\theta_0 = 30°$. (*b*) Superposition of four successive photographs of its destabilization. On the last picture the secondary branch has stopped growing. The tip-splitting instability is imperfect.

cell with the square of the length scale of the destabilization. Secondly it is preceded by a very small prefactor. As the Saffman–Taylor finger grows, its tip becomes wider and looks more and more similar to a plane front. With such an argument, one would expect that a finger destabilizes, in a first approximation, as a plane front on a characteristic scale on the order of l_c. For this reason we thought it useful to introduce a new parameter ω defined as the ratio of the finger width at the tip approximated by λW_T to the capillary length scale:

$$\omega(\theta) = \lambda W_T / l_c. \tag{3}$$

It is related to B by

$$\omega(\theta) = \lambda(8.45 \times 10^{-3}/B)^{0.5}. \tag{4}$$

From the theoretical values of λ and $B_{th}(\theta_0)$ calculated by Ben Amar *et al.* (1991), we calculated the theoretical value ω_{th} at the onset of destabilization. The corresponding

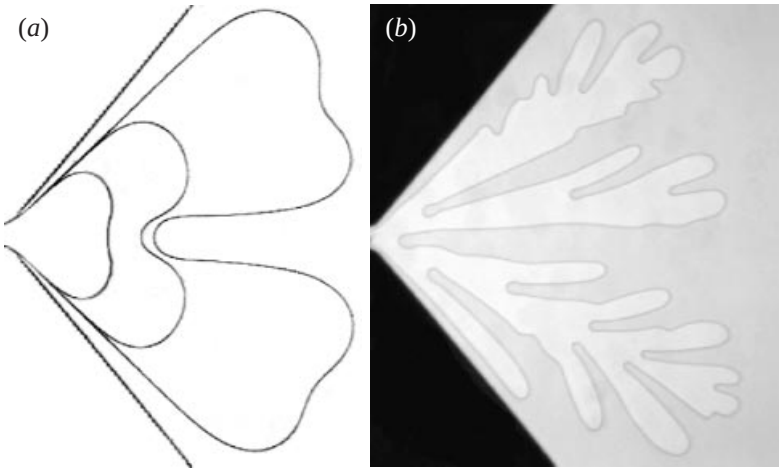

FIGURE 3. (*a*) Superposition of three successive photographs of the destabilization of a Saffman–Taylor finger in a sector-shaped cell of angle $\theta_0 = 100°$. (*b*) The corresponding developed pattern. The two branches generated by the instability keep growing independently and form two large-scale structures. The tip-splitting instability is perfect.

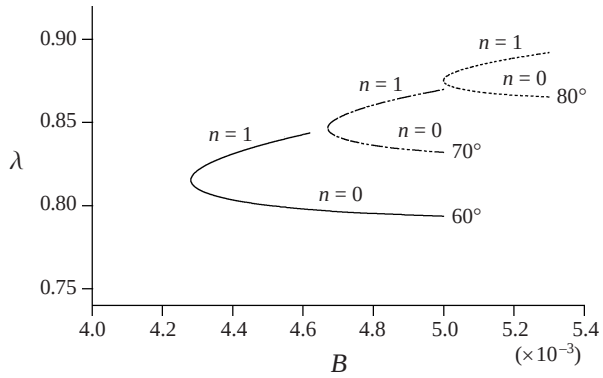

FIGURE 4. The coalescence of the two lower branches ($n = 0$ and $n = 1$) of the discrete set of solution as obtained numerically for three wedges of angle $\theta_0 = 60°, 70°$ and $80°$ respectively.

curve, plotted on figure 6, diverges when θ_0 decreases so that $\omega_{th}(0) = \infty$. From our experimental measurements we can also deduce the value ω_{ex} of ω at the onset of destabilization. These values are compared to the theoretical predictions on figure 6.

We can now use figures 5(*b*) and 6 to discuss the theoretical results in physical terms and to compare theory and experiment.

For the linear channel, the theory predicts the linear stability of the Saffman–Taylor finger up to $\omega = \infty$ (or down to $B = 0$). In fact, the strong curvature at the finger tip in this particular geometry has a stabilizing effect because the disturbances do not have time to grow. They are advected away from the unstable front region towards the rear of the finger where the normal velocity (and therefore the perturbation growth rate) vanishes. This process was investigated numerically by Park & Homsy (1985) and De Gregoria & Schwartz (1986).

However, experimentally, as observed by Tabeling *et al.* (1987), the fingers become unstable above a threshold of the order of $\omega_{ex}(0) = 4$ (or $B = 1.4 \times 10^{-4}$). This difference between theory and experiment can be ascribed to a nonlinear destabilization

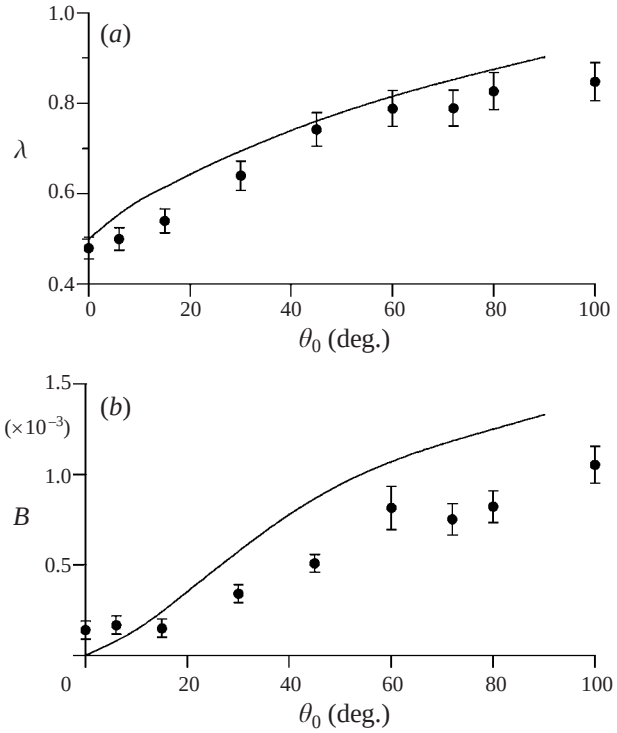

FIGURE 5. (*a*) The relative finger width λ at the onset of destabilization as a function of the cell angle θ_0. The curves correspond to the theoretical predictions of Ben Amar *et al.* (1991) and the dots to our measurements. (*b*) The value of the parameter B at which the finger destabilizes as a function of the cell angle θ_0.

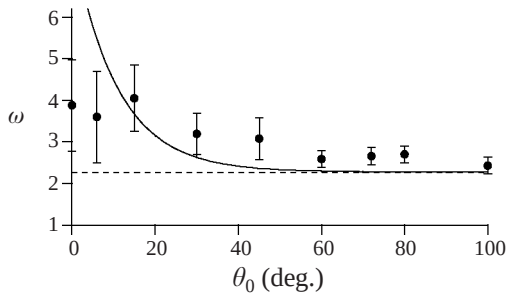

FIGURE 6. Finger tip width normalized to the capillary length ω at the onset of destabilization as a function of the cell angle θ_0. The curve shows the theoretical predictions of Ben Amar *et al.* (1991) and the dots our measurements.

of the finger triggered by small but finite disturbances due to the imperfections of the cell. The initial amplitude of the perturbation is an important parameter in the competition between the growth time and the advection time as demonstrated by Bensimon (1986). The values we found experimentally were in agreement with those of Tabeling *et al.*; they correspond to the natural disturbances in a cell with clean glass plates. If noise is added, smaller values of $\omega_{ex}(0)$ are found.

In divergent wedges the tip is flatter and the advection weaker so that the stabilizing effect of curvature decreases rapidly with the increase of the angle. For wedges of

angle $\theta_0 > 60°$, an asymptotic value of approximately $\omega_{max} = 2$ is reached. In other words, for large wedges, as soon as the width of the finger becomes of the order of $2l_c$, it becomes unstable. This gives an intuitive understanding of the existence of the theoretically computed loops and of the limit they impose on the finger stability. For these wedges the agreement between experiment and theory is good (figures 5*b* and 6) with however a slight systematic shift towards larger values of the experimental measurements ω_{ex}. This can be ascribed to the fact that theory predicts the exact moment of the finger destabilization whereas experimentally one has to wait for the perturbation to be large enough to distinguish a finite flattening in the finger profile.

4. Shape of the fjords

4.1. *Study of the shape of the central line of the fjords*

The flat, which is the first visible sign of a finger's destabilization, rapidly becomes an indentation, in the centre of which the interface stops moving (figures 2*b* and 3*a*). This local inversion of curvature thus marks the beginning of the splitting of the initial finger in two branches. These two branches are separated by a region, which we will call a fjord, in which the oil remains blocked (figures 2*b* and 3).

Investigating the later evolution of this splitting instability, we observed that this process can lead to two different kinds of long-term behaviour. In the first case, observed for all angles $\theta_0 < 70°$ (including the linear channel), the instability fails to create two independent long-lived structures. One of the branches, which we will call the secondary branch, is ejected from the side of the finger and stops growing (figure 2*b*). The other branch, which we will call main branch, widens increasingly and will tend to become unstable again. In the following, this process will be referred to as 'imperfect tip splitting'. In the second case, observed in cells of large angles ($\theta_0 > 90°$), both branches keep growing independently (figures 3*a* and *b*) and form long-lived structures. We will refer to this latter case as 'perfect tip splitting'.

The transition between these two kind of behaviour occurs in the intermediate range $70° < \theta_0 < 90°$, where both perfect and imperfect tip splitting can be observed. It is worth noting that this transition zone corresponds approximately to the range where the parameter ω reaches its limiting value $\omega_{th} = 2$.

The possibility of the existence of a critical angle in Laplacian growth has already been discussed, especially in the context of DLA (Argoul *et al.* 1990; Arnéodo *et al.* 1989). These theoretical studies suggested the existence of a five-fold symmetry, corresponding to the critical angle $\theta_c = 4\pi/5 = 144°$. More recently, Kessler *et al.* (1998) also found theoretically the existence of a critical angle $\theta_c = 120°$–$140°$. Their study predicts that for angles larger than θ_c, two branches can coexist and form long-lived structures. Our experiments seem to confirm the existence of such a critical angle but with a value smaller than that predicted by Kessler *et al.* We must note that the value of this angle is probably underestimated in our experiments because the patterns we studied were not very large and what we estimated to be long-lived structures may still have stopped if we could have let the pattern grow larger.

4.2. *A model for the shape of the central line of the fjords*

To put these observations on a more quantitative footing it turns out that it is more appropriate to study the shape of the fjords instead of that of the secondary branches. In fact perfect tip splitting always corresponds to radial fjords with their axis passing through the cell's apex (figure 3). On the other hand, in the imperfect tip splitting case, the fjords observed are curved. Their initial axis is always somewhat divergent

from the cell's axis (figure 2*b*) and with time this axis rotates progressively further away from the cell's axis until the side finger stops growing.

In order to understand this evolution, we propose an interpretation based on the two following hypotheses:

(i) The destabilization of the Saffman–Taylor front occurs by the amplification of a motionless disturbance, i.e. one having no intrinsic propagation. Its only motion is due to its advection along the curved profile, a kinematic effect pointed out by Zel'dovich (1980) (see also Pelcé 1988).

(ii) The formation of an indentation in the interface, being very local, only affects the nearest of these isobars. The further ones remain undisturbed and tend to stabilize an envelope of the structure similar in shape to the stable finger. In other words, the structure formed of the main branch and the lateral branch retains a memory of the previous stable structure.

With these two hypotheses, the evolution of the fjords separating the two branches can be predicted from the evolution of the finger had it remained stable. More precisely, we shall show that the shape of the fjord is similar to the trajectory of a point of the interface that would be on a stable Saffman–Taylor finger. This trajectory is particularly easy to determine as it is given by the curves normal to the successive finger profiles.

4.2.1. *Case of the linear channel*

We first consider a stable finger moving in a linear cell with a velocity U relative to the laboratory frame. The x-axis corresponds to the cell's axis. The origin is chosen so that the coordinates of the tip at a given time t are $x = Ut$ and $y = 0$. With these conventions, the shape of the stable finger at a given time t found by Saffman & Taylor in the absence of surface tension is

$$x - Ut = f(y) = \frac{W(1-\lambda)}{\pi} \ln\left[\cos\left(\pi y/\lambda W\right)\right]. \tag{5}$$

Computing the components of the normal vector, we get

$$n_x = \frac{1}{\sqrt{1+(\mathrm{d}f/\mathrm{d}y)^2}}, \quad n_y = \frac{-\mathrm{d}f/\mathrm{d}y}{\sqrt{1+(\mathrm{d}f/\mathrm{d}y)^2}}. \tag{6}$$

A small displacement $\mathrm{d}l = (\mathrm{d}x, \mathrm{d}y)$ of a particle advected with the interface must be parallel to the normal direction. This implies

$$\mathrm{d}x = \frac{n_x}{n_y}\mathrm{d}y = \frac{\lambda}{(1-\lambda)} \frac{\mathrm{d}y}{\tan\left(\pi y/\lambda W\right)}. \tag{7}$$

Integrating equation (7), we find that the trajectory of a disturbance initially located at the point (x_s, y_s) is described when $0 < y_s < \lambda$ by the equation

$$x - x_s = \frac{W\lambda^2}{\pi(1-\lambda)} \ln\left[\frac{\sin\left(\pi y/\lambda W\right)}{\sin\left(\pi y_s/\lambda W\right)}\right]. \tag{8}$$

In the particular case where $y_s = 0$, the trajectory is the straight line $y = 0$.

The trajectories corresponding to two different starting points on a finger of width $\lambda = 0.5$ are plotted on figure 7(*a*). The fjord length l_f is larger when its starting point is closer to the finger tip, a property that had already been noticed by Kopf-Sill & Homsy (1988). However, in both cases, the fjord axis bends progressively until the perturbation is finally convected to the side of the finger, where it stops moving. This fact is more evident on figure 7(*b*) which shows the normal trajectories starting from

initial points located at regular intervals along the finger profile. The fjord length l_f diverges when its starting point reaches the finger tip. However, all the trajectories are finally convected to the finger side except that issuing from the finger tip itself. This latter trajectory is singular, being a straight line parallel to the wall.

Finally, it is worth noting that all the normal curves (but the one issuing from the finger tip) are parts of identical curves simply translated along the cell's axis. This property is a consequence of the translational invariance of the Saffman–Taylor finger in linear geometry. It is worth noting that these curves have exactly the same shape as the finger itself but translated a distance $y = \lambda/2$ along the y-axis. To our knowledge, this property of Saffman–Taylor fingers had remained unnoticed up to now.

4.2.2. *Case of the wedges*

In the case of wedges, the successive profiles are self-similar. Although their analytical expression is known (Ben Amar 1991), it is given in terms of hyper-geometric functions which are difficult to manipulate. For this reason we chose to compute numerically the normal trajectories using the following procedure. For each angle θ_0, we get the profile of the finger having the limit width λ_θ as obtained by numerical simulation. This profile was interpolated using the cubic spline method in order to get a large number N of points on the interface. A starting point being chosen on this profile, we computed the normal vector coordinates at this initial point. The finger was then propagated by one step. Because of the interface auto-similarity, this was simply done by expanding the finger by a factor $(1 + \varepsilon)$. The new position of the particle was given by the intersection of the normal with the new profile. This procedure was iterated as many times as needed. The precision of this calculus depends both on the number N of points at the interface and on the expansion factor ε. The unit of length being given by the finger length, we obtained good results with $N = 50\,000$ and $\varepsilon = 0.01$. The N points were not set uniformly on the interface. Their density was increased in the vicinity of the tip where the trajectories lengths change more rapidly. As in the linear case, the point stops moving when it has been convected to the side of the finger where the advection velocity is zero.

The trajectories corresponding to two different starting points on a finger of width $\lambda = 0.815$ in a wedge of angle $\theta_0 = 60^\circ$ are plotted on figure 8(*a*). Figure 8(*b*) shows a set of trajectories originating from equidistant points along the finger profile. The fjord length diverges to infinity when the starting points get closer to the tip. As in the case of the linear geometry, all the trajectories but one correspond to a rejection on the side of the finger. The exception is the trajectory originating from the tip, which is a straight line along the axis of symmetry of the cell.

It is also worth noting that all the trajectories can be deduced from one another by applying a scaling factor. This property is a direct consequence of the self-similarity of Saffman–Taylor fingers in wedges.

4.3. *Comparison of the central line of the fjords to the shape of the normal curves*

In order to compare the experimentally observed fjords to the calculated trajectories we used video tape recordings of the finger evolution. For the second hypothesis of § 4.2 to be valid we must start from undisturbed fingers and observe their destabilization.

In a linear channel however, ω remains constant during the growth of a finger. Therefore a given experiment leads either to a stable or to an unstable finger. This is the reason why in the case of linear channels we limited ourselves to weakly unstable fingers where the finger remains close to a stable one. A more general investigation is

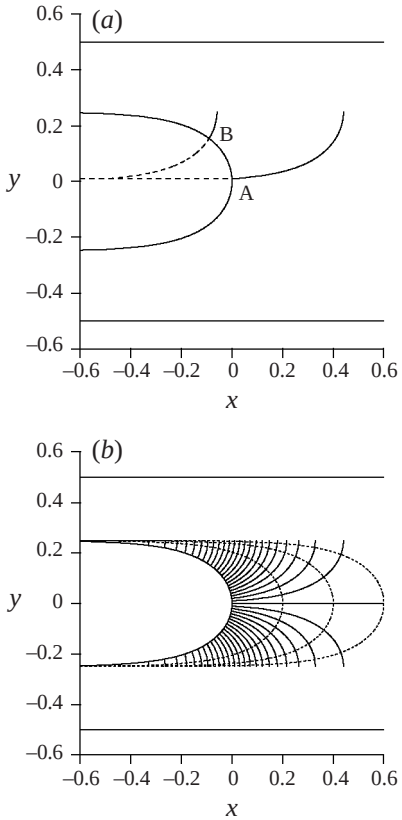

FIGURE 7. (*a*) Trajectories of two points A and B of a finger profile of width $\lambda = 0.5$ in a linear cell. (*b*) Set of trajectories issued from equidistant points along a Saffman–Taylor finger front.

possible in wedges. The reason is that if the finger velocity is constant the growth in this geometry is always stable near the apex. We simply let this stable finger grow. As W increases B decreases and we observe the finger's first destabilization. Rewinding the tape we seek the first image where an indentation is observed in the finger tip region. We then use the theoretical array of normal curves in the wedge of angle θ_0 (of the type shown on figures 7*b* and 8*b*). We adjust the figure scale so that the theoretical finger fits the experimental one at the stage where it destabilizes. We then choose the normal curve having its starting point in the centre of the indentation. If our hypotheses are justified this curve should give the central line of the fjord observed later. The results of such fits are displayed on figure 9 for the linear channel case and figures 10, 11 and 12 for wedges of angle respectively $\theta_0 = 30°, 60°$, and $100°$.

The prediction, though not perfect, is a good enough approximation. In particular in all the cases where the secondary branch has stopped growing (figures 9 and 10) it is observed to be neatly enclosed inside the curved trajectory. This means that knowing the origin of a disturbance it is possible to predict where the secondary branch will stop. This characteristic is at the origin of the generalization of the virtual walls presented in the next paragraph.

The experimental results depart from what is expected in two ways. For the linear channel and the wedges of small angles the observed fjords appear less bent than predicted (figures 9 and 10). The main reason for this is that when the trajectory

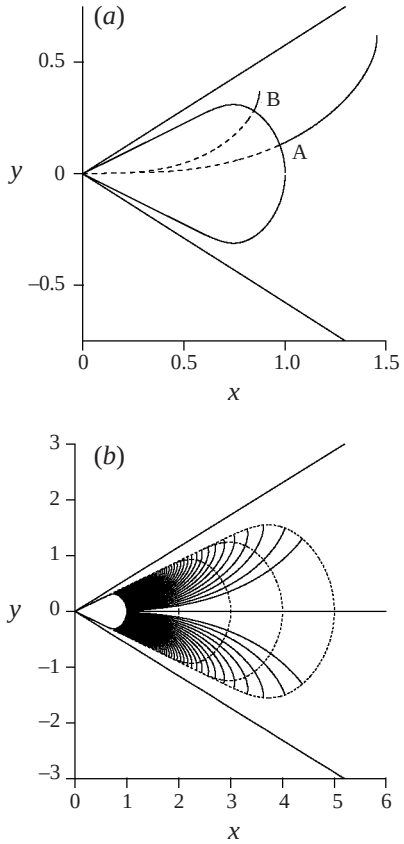

FIGURE 8. (*a*) Trajectories of two points A and B of a finger profile of width $\lambda = 0.815$ in a sector-shaped cell of angle $\theta_0 = 60°$. (*b*) Set of trajectories issued from equidistant points along a stable finger of length $r_T = 1$.

bends towards the wall the secondary finger simply stops growing so that the part of the fjord corresponding to the most lateral part of the trajectory remains virtual.

A second limitation is observed for very unstable fingers in linear channels. It is known (Arnéodo *et al.* 1989) that their ensemble average statistically reproduces the shape of the stable finger. However one given realization can have an envelope that departs from that shape. In particular, a given finger can grow for some time on one side of the channel. Evidently, in all these cases the fjords cannot be compared to the normal trajectories to the symmetrical finger. However, as we will see, the length repartition of the weakly unstable fingers retains statistical validity for the branches of very unstable fingers.

4.4. *Generalization of the notion of virtual wall and application to the description of the secondary branches*

The shape of the fjords being known, the next question which arises concerns the shape of the two branches growing on each side of the fjord. Let us recall that, in the case of a circular cell, the destabilization of an initial circular front leads to the formation of five or six fingers growing between radial fjords. Thomé *et al.* (1989) observed experimentally that these fingers grow as if enclosed in virtual wedge-shaped cells, the walls of which correspond to the central line of the fjords.

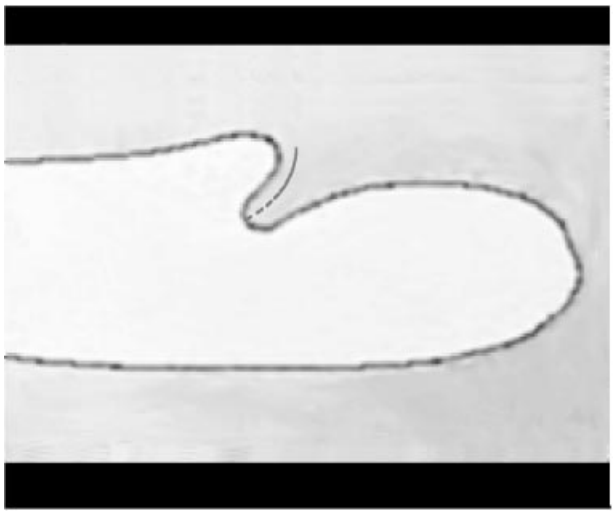

FIGURE 9. In a linear channel the typical instability observed near the instability threshold is a very imperfect tip splitting. The photograph is taken when the secondary branch has stopped growing. The dashed line is the normal curved passing through the point of initial destabilization.

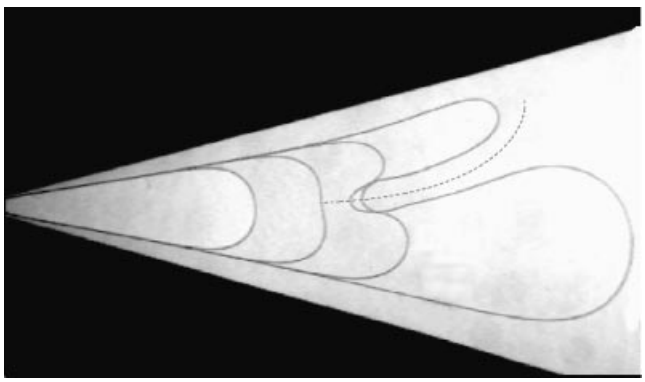

FIGURE 10. The dynamics of an imperfect tip splitting in a wedge of angle $\theta_0 = 30°$. The figure shows the superposition of four successive profiles. The flattening corresponding to the initial destabilization is seen on the second profile. On the fourth profile the resulting secondary finger has stopped to grow. The dashed line is the normal curve passing through the point of initial destabilization.

The destabilization of fingers in wedges is very similar to the first destabilization in circular cells: stop points form leading to the formation of fjords in which the fluid remains motionless. For this reason, we tried to generalize the procedure and to identify the central lines of the fjord with a virtual wall. Each of the two branches resulting from a splitting instability therefore grows as if confined between a real wall (one of the cell wall) and a virtual wall (the fjord) (figures 9 to 12).

The simplest situation corresponds to the perfect tip splitting observed for large wedges $\theta_0 > 90°$ (figure 12). In this case the virtual wall is radial and divides the initial cell into two parts. Each of the two branches grows in a virtual divergent wedge of angle $\theta_0/2$. As they keep growing, both secondary branches will become progressively wider until they destabilize again (figure 12). During this destabilization the fjord axis retains its shape.

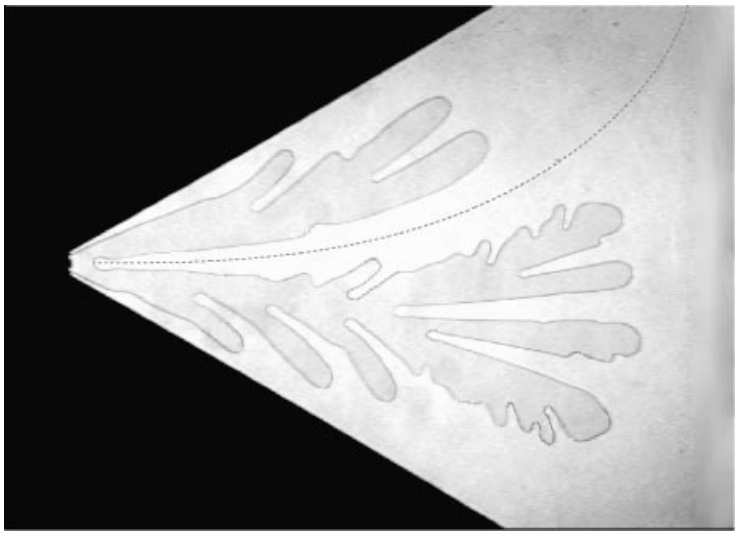

FIGURE 11. Case of a very large fjord formed in a wedge of angle $\theta_0 = 60°$. Comparison between the calculated trajectory (dashed line) and the experimentally observed fjord. Note that the fit is good even though the secondary branches themselves undergo secondary destabilizations. On this image, the secondary branch has not yet stopped growing.

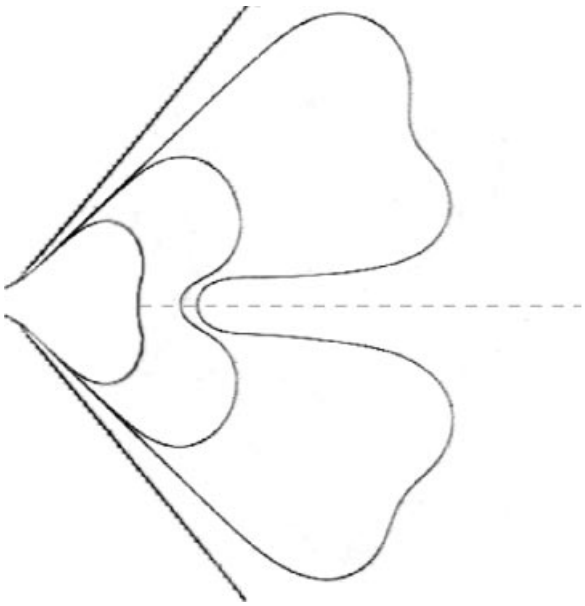

FIGURE 12. Comparison between the calculated trajectory (dashed line) and the experimental observed fjord for a perfect tip-splitting in a wedge of angle $\theta_0 = 100°$.

In narrow cells ($\theta_0 < 70°$), as stated above, no perfect splitting is observed. Instead an imperfect splitting occurs forming a curved fjord (figures 9 to 11). The fjord being curved, each branch grows in virtual channels one of the lateral walls of which is curved. This type of channel has never been investigated so that the evolution of a finger in such a cell cannot be precisely predicted. However, the growth in normal wedges is mainly sensitive to the structure of the boundaries in the region of the tip. It

is thus possible, in a first approximation, to replace a curved wall by the straight wall tangent to it in the region where the growth occurs. In this approximation, at a given time, the two branches resulting from a tip splitting both move in two virtual wedges. The tip splitting being imperfect, these two virtual cells are however very different (figures 9 to 11). Due to the curvature of the virtual wall, the wider cell becomes more divergent. As a result, the main branch widens increasingly and will tend to become unstable again. In contrast, the narrower cell becomes more convergent (with $\theta_0 < 0$) and heads into a dead end because it moves towards the wall of the real cell. As a result, the corresponding finger becomes narrower and stops growing (figures 9 and 10) roughly when it reaches the envelope of the stable structure of the initial cell (well before it would have collided with the cell wall).

5. The size distribution of the fjords and of the secondary branches

With these assumptions the shapes of the main and secondary branches can be interpreted well if the position of the initial disturbance is known. The length of a fjord being critically sensitive to the position of the initial dip, there is a direct link between this length and the structure of the stable finger tip. As a result the tip-splitting process appears, by itself, to be able to generate fjords and side branches of all sizes. However, at this stage it does not explain why perfect tip splitting dominates at large angles whereas only imperfect tip splitting is observed at small angles. In this section, we will examine in more detail the length l_f of a trajectory (and thus of a fjord) as a function of the position $s(x_s, y_s)$ of its starting point. Assuming a homogeneous distribution of the starting points and taking into account the effect of the width of the perturbation as compared to the finger width, it is possible to predict the fjord size distribution. We will thus reach a qualitative understanding of the transition from imperfect to perfect tip splitting.

5.1. *Fjord size distribution in linear channels*

Let us first consider the case of the linear cell. Taking advantage of the symmetry of the finger, the following calculations were performed on half of the profile. The probability distribution function $f(l_f)$ of the trajectories of size l_f is related to the probability distribution function $g(y_s)$ of the transverse position of the starting point by

$$f(l_f)\,\mathrm{d}l_f = g(y_s)\,\mathrm{d}y_s. \tag{9}$$

Let us assume that the main source of destabilization of the fingers comes from point-like defects of the glass plates homogeneously distributed across the channel width. In that case, the disturbances impinging on the interface have a constant density in the direction transverse to the cell. For these reasons, we will assume a constant probability distribution function for the transverse position of the disturbance $g(y_s)$ and calculate $f(l_f)$ from the equation

$$f(l_f) = g(y_s)\left|\frac{\mathrm{d}y_s}{\mathrm{d}l_f}\right|. \tag{10}$$

In the case of the linear geometry, the length of a trajectory originating from a point at the interface of ordinate y_s is

$$l_f = \int_{y_s}^{\lambda W/2} \sqrt{1 + (\mathrm{d}x/\mathrm{d}y)^2}\,\mathrm{d}y, \tag{11}$$

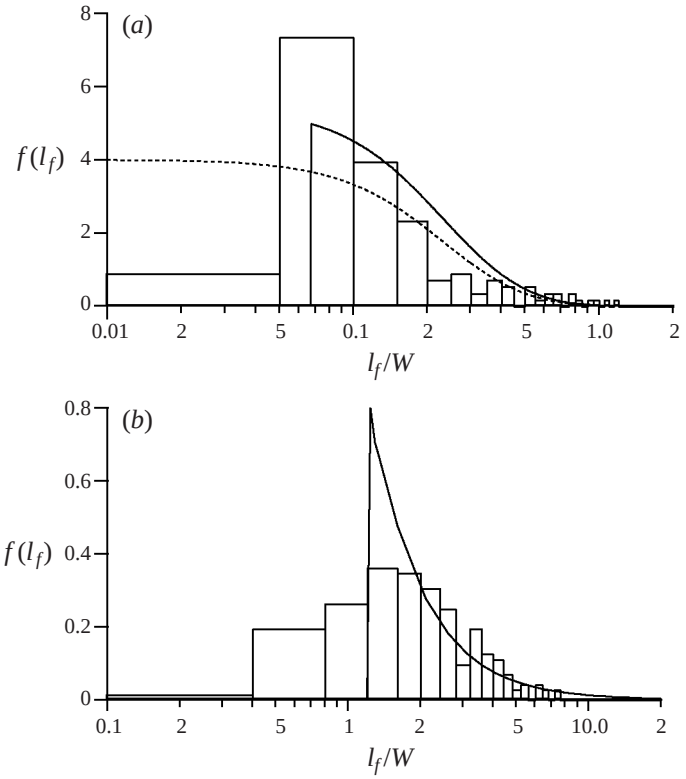

FIGURE 13. (*a*) Probability distribution function of the fjord lengths in the linear geometry ($\theta_0 = 0°$); boxes, experimental results; dotted line, homogeneous distribution of all the defects (equation (13)); continuous line, disturbances in the central band only (equation (14)). (*b*) Probability distribution function of the fjords lengths in a wedge ($\theta_0 = 45°$). Boxes: experimental results. The continuous line is the distribution computed numerically.

where l_f is normalized with respect to the cell width and x and y are linked by equation (8). Integrating this equation in the case of a finger of width $\lambda = 0.5$, we get

$$l_f(y_s) = -\frac{W}{2\pi} \ln [\tan (\pi y_s/W)], \tag{12}$$

so that the probability distribution function of having a fjord of length l_f is

$$f(l_f) = \frac{4}{W} \sin [2 \tan^{-1}(e^{-2\pi l_f/W})]. \tag{13}$$

In order to obtain an experimental distribution, we performed measurements of the fjord lengths in a linear cell in repeated experiments. The resulting histogram corresponding to 150 independent runs provides the probability distribution function shown on figure 13(*a*). The agreement between the experimental distribution and the predicted one (dotted line on figure 13*a*) is reasonably good for long branches. However, the number of small branches is greatly overestimated. In fact, one observes experimentally the existence of a kind of cut-off length of the order of $0.05W$, below which the probability of observing branches becomes very small.

The existence of this cut-off length can be understood qualitatively in the following

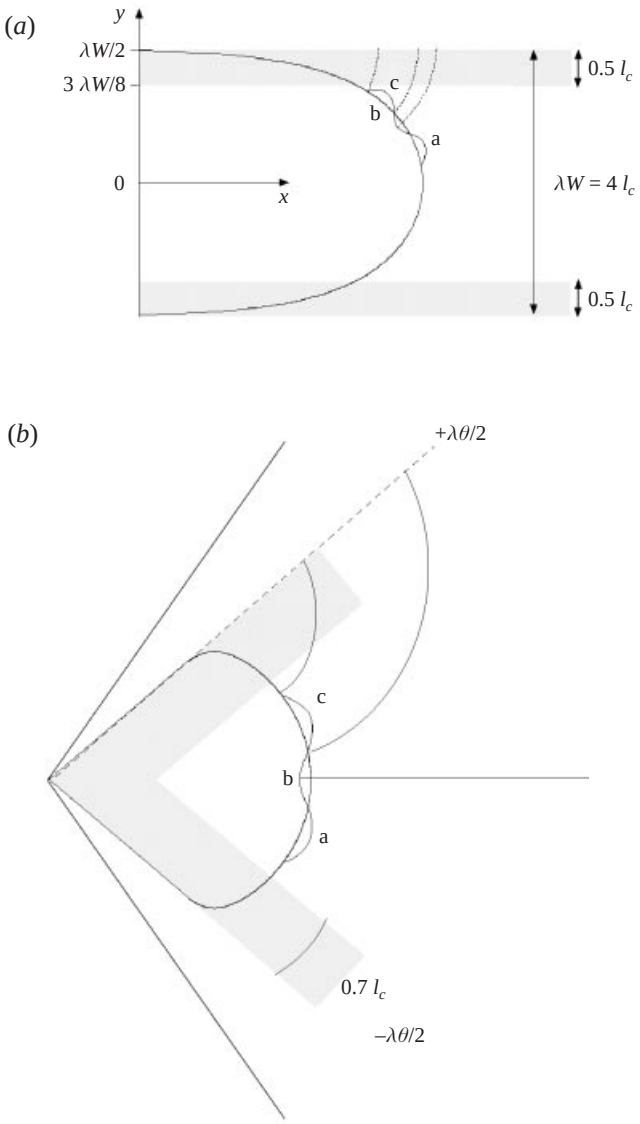

FIGURE 14. (*a*) Schematic of the possible positions of the wavepacket of a disturbance and of its evolution in the linear channel. Because of the necessary extent of the wavepacket the disturbances located in the two grey bands are not efficient in destabilizing of the finger. (*b*) The same schematic for a large-angle wedge.

way. The initial perturbation is likely to be point-like. However, due to surface tension the resulting observed disturbance of the front appears as a wavepacket, formed of an indentation separating two bumps (figure 14*a*). The wavelength of this wavepacket is roughly of the order of the local capillary length scale. In the tip region this local length is always close to the value l_c associated with the finger tip velocity. The bumps are the precursors of the main and secondary branch while the indentation is that of the fjord. Because of the bumps, the fjord starting point cannot be located far back on the finger side. This implies the existence of a forbidden zone on the stable

Saffman–Taylor finger from where no fjord can start as schematized on figure 14(*a*). Secondary branches corresponding to fjords which would start from this forbidden zone are therefore never observed. This simple image can be made more precise. As seen in § 3, the finger width, λW, in linear cells is of the order of $4l_c$ at the onset of destabilization ($\omega_{max} \sim 4$). The wavepacket width being of the order of l_c, the range of possible starting points for the fjord is relatively important, depending on the position of the perturbation on the finger.

The complete analysis would be complex because it is necessary to take into account the stretching due to the kinematics of the front as analysed by Zel'dovich (1980) as well as the shift of the local unstable wavelength due to the decrease of the local normal velocity as shown by Caroli, Caroli & Roulet (1987) in the case of dendritic crystals. We will limit ourselves here to a qualitative argument. In a first approximation the three parts of the wavepacket, labelled a, b, c on figure 14(*a*) are advected along normal lines. It can be seen that the stretching by the advection decreases going from a to c. If the bump c is located too far on the side of the finger its length will very rapidly be too short to correspond to one of the locally amplified wavelengths. This is experimentally observed: when a disturbance occurs too far from the finger's axis it fails to generate a lateral branch because part c of the wavepacket is not amplified.

Experimentally, the cut-off length is observed to correspond to a fjord starting point located $0.5l_c$ from the finger side. In other words, the forbidden zone corresponds to points of ordinate $|y_s| > 3\lambda W/8$. *A contrario* all the disturbances having their centre located nearer to the finger axis generate a splitting. This effect can be taken into account by assuming a constant probability distribution function for the transverse position of the disturbance $g(y_s)$ in the interval $|y_s| < 3\lambda W/8$. This leads to the following expression for the secondary branch size probability distribution function:

$$\left.\begin{aligned} f(l_f) &= \frac{16}{3W}\sin\left[2\tan^{-1}\left(\mathrm{e}^{-2\pi l_f/W}\right)\right] \quad \text{for} \quad l_f > l_0, \\ f(l_f) &= 0 \qquad\qquad\qquad\qquad\qquad\quad \text{for} \quad l_f < l_0, \end{aligned}\right\} \tag{14}$$

where l_0 is the length of a branch originating from a point of ordinate $|y_s| = 3\lambda W/8$, given by

$$l_0 = -\frac{W}{2\pi}\ln\left[\tan\left(\frac{3\lambda\pi}{8}\right)\right]. \tag{15}$$

This distribution is shown (continuous line) on figure 13(*a*) and gives a good fit to the experimental p.d.f. An interesting result is that the probability of having fjords larger than the cell width W is very small. In particular, though perfect tip splitting does not seem *a priori* to be excluded, their probability is negligible.

Two remarks can be made.

It should be noted that the derivation of the size of the forbidden zone relies on the observation that $\omega_{ex}(0) = 4$ (or $B = 1.4 \times 10^{-4}$) at the onset of destabilization. However, as already mentioned, the value of B and therefore of ω at the onset of destabilization in a linear cell depends on the noise level in the particular experiment (Bensimon 1986 and Tabeling *et al.* 1987). As a result, the size of the forbidden zone and the resulting fjord size p.d.f. should also depend on the noise level. This was not investigated.

As stated in § 4.3 the strongly unstable fingers can be asymmetrical. In this case the side branches growing on the side where the cell is wider can be slightly longer. Statistically however, the distribution found above retains its validity.

5.2. *Fjord size distribution in wedges*

As in the case of the linear channel, we also performed repeated measurements of the secondary branch length in wedges of varying angles. Figure 13(*b*) displays the resulting probability distribution function obtained by 200 independent measurements in a wedge of angle $\theta_0 = 45°$. There is again a cut-off length at small scales which is now of order W. The probability of observing branches smaller than that is very small.

Considering, as above, the disturbance as a wavepacket formed of two protrusions separated by an indentation and having a total length of the order of $1.5l_c$, the finger destabilization in wedges is schematized on figure 14(*b*). It can be noted that in wedges of large angle, λ being very large, the front of the finger is not very different from an arc of a circle so that its local velocity does not vary much over the whole front part. As a result the local capillary length l_c can be considered as constant. The experimentally observed cut-off length for $\theta_0 = 45°$ corresponds to a fjord starting point located $0.75l_c$ from the finger side. In other words, the width of each of the forbidden zones is of the order of $0.75l_c$. This observation, confirmed by another series of experiments in angular sectors of angle 30° and 60°, confirms that the perturbation width is of the order of $1.5l_c$. Note that in the sector geometry, the value of ω at the onset of destabilization and therefore the size of the forbidden zone do not depend on the noise level.

In the case of wedges, the initial disturbance of the finger is characterized by its angular position θ_s. The distribution of the trajectory lengths $f(l_f)$ is related to the distribution of positions of the initial disturbance $g(\theta_s)$ by

$$f(l_f) = g(\theta_s)\left|\frac{\mathrm{d}\theta_s}{\mathrm{d}l_f}\right|. \tag{16}$$

Assuming a constant angular distribution $g(\theta_s)$ of the disturbances outside the forbidden region, we calculated numerically the fjord size distribution. The computed fjord size distribution function is compared to the experimental histogram in figure 13(*b*). Taking into account the simplicity of our model, the agreement is rather good. Figure 13(*b*) shows that for $\theta_0 = 45°$ the most probable size for the branches is of the order of W and thus much larger than in the linear case.

The observation that the perturbation width is of the order of $1.5l_c$ is an interesting result. As noted in § 3, the finger width at the destabilization normalized by the capillary length, $\omega_{max}(\theta_0)$, decreases when the sector angle θ_0 increases. For angles θ_0 larger than 60°, $\omega_{max}(\theta_0)$ becomes on the order of 2. Therefore a disturbing wavepacket of width on the order of $1.5l_c$ has to hold onto a finger tip, the width of which tends towards $2l_c$ at large angles. As a result, the indentation and therefore the fjord starting point become more and more confined to the vicinity of the finger tip. This effect enhances the probability of long branches and could therefore give a physical meaning to the transition from imperfect to perfect tip splitting which occurs between $\theta_0 = 60°$ and $\theta_0 = 90°$. This analysis, however, does not lead to a precise value of a critical angle for the transition from imperfect to perfect tip splitting.

6. Description of complex patterns

6.1. *Application of the notion of virtual wall*

Until now, we have only considered the first destabilization of a Saffman–Taylor finger. The secondary branches issuing from the destabilization can themselves destabilize, creating a second generation of branches and so on. We can now try to generalize

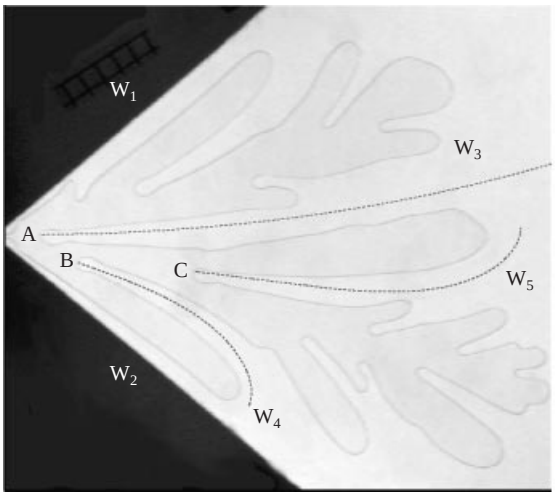

FIGURE 15. A complex pattern obtained in a $\theta_0 = 80°$ cell, showing a hierarchy of virtual cells. The finger enclosed between W_2 and W_4 has stopped growing. The finger located and between W_3 and W_5 has practically stopped. The structures between W_1 and W_3 and between W_4 and W_5 are still growing.

the previous results to the next generations of branching. Figure 15 shows a complex pattern observed in a wedge of angle $\theta_0 = 80°$.

The first destabilization occurs at point A in the real cell composed of real walls, labelled W_1 and W_2 on figure 15. This is an imperfect tip splitting which gives rise to a fjord labelled W_3. The shape of W_3 is fitted very well by the theoretical calculated curve shown on figure 15 computed in the usual way (for a wedge of angle $\theta_0 = 80°$).

As discussed in § 4.4, the fjord central line W_3 forms a virtual wall. We can now consider the secondary branch growing confined between walls W_2 and W_3. In the region where this finger destabilizes, the virtual cell formed by W_2 and W_3 can be approximated by a normal wedge of angle $\theta_0' = 40°$. In this approximation it is possible to predict the radial position of B, the point where the finger destabilizes and to fit the shape of the resulting new fjord W_4.

This process can be repeated with the finger growing between the two virtual walls W_3 and W_4. It splits in C and forms a new fjord W_5. The shape of W_5 can be predicted by approximating the virtual cell formed by W_3 and W_4 by a wedge of angle $\theta_0'' = 30°$. This procedure could be generalized to the description of all splittings but the situation becomes more and more intricate so that the shapes of the virtual cells are more and more complex, having for instance more than two curved walls.

6.2. *Reproducibility of complex patterns*

Several observations led us to think that if identical initial destabilizations were obtained there was a sort of length of persistence. In other words, after a reproducible first branching the evolution of the pattern became deterministic for some time. In order to test this idea we performed a series of experiments aimed at testing the reproducibility of the successive branchings when the first one was fixed. For this purpose, instead of letting the finger destabilize spontaneously, the first instability is artificially triggered by a local perturbation in the cell. This was obtained by placing a finite protrusion on one of the lateral walls (see figure 16). The disturbance was placed a little nearer to the apex than the position of spontaneous destabilization

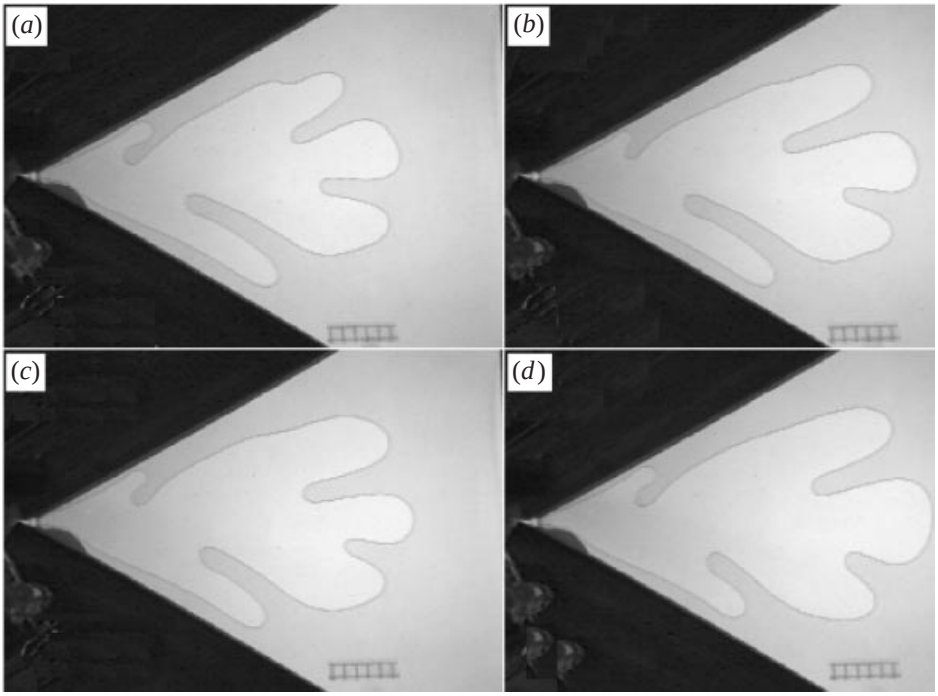

FIGURE 16. Four patterns obtained in identical experimental conditions in a $\theta_0 = 60^\circ$ cell. The first tip splitting has been triggered by the bump in the lateral wall visible on the photographs.

of the finger at the chosen velocity. Passing in front of this protrusion, the finger becomes asymmetric and its destabilization is biased: a lateral branch is formed on the opposite side of the disturbance. The next branch appears on the other side and this process repeats itself. We present as an example on figure 16 the patterns obtained in four different realizations for the same conditions in a 60° cell. The pattern is surprisingly reproducible. The whole behaviour of the finger looks oscillatory though the periodicity is still not very well determined. If the conditions of injection are maintained strictly identical the pattern formed by the first four or five side branches form in a deterministic way. Note that this kind of oscillating pattern also observed by Park & Homsy (1985) is not a direct consequence of the lateral disturbance as we also observed it to occur spontaneously.

7. Discussion and conclusion

We can now revisit the axisymmetric growth in the radial geometry. Figure 17 shows two patterns corresponding to different stages of the growth. On figure 17(*a*) are shown the first two stages of destabilization. The walls formed during the destabilization of order zero are radial and they appear to extend to infinity. Indeed, on figure 17(*b*) a well-developed pattern is observed to remain separated in the sectors defined initially. This means that as the structure expands, the 'memory' of the initial disturbance is kept. The pressure field being Laplacian, the scale on which it is disturbed in the radial direction is of the same order of magnitude as the scale of the disturbances of the interface in the azimuthal direction. The azimuthal disturbances of largest scales always correspond to the division into sectors which occurred initially. For this reason they are the disturbances which disturb the furthest isobars. As the structures grow,

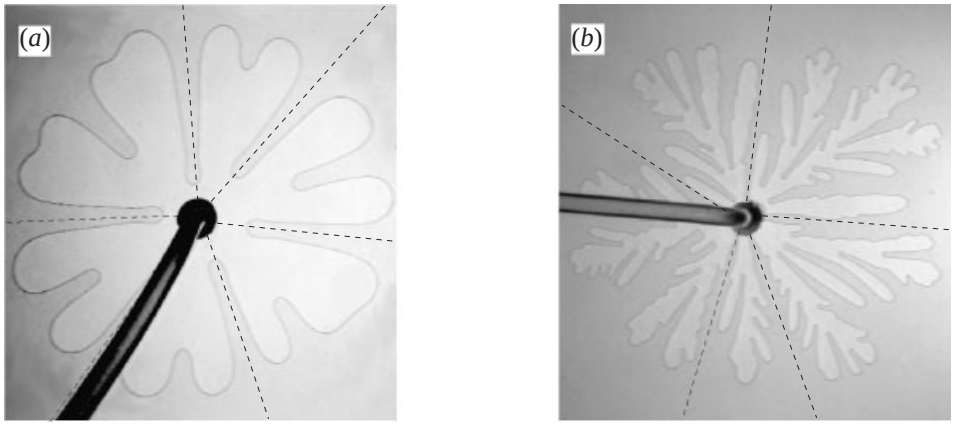

FIGURE 17. Two patterns obtained in a circular geometry, showing the role of the virtual cells (*a*) at an early stage of the growth and (*b*) for a more developed pattern.

isobars located further and further away will be affected. These isobars thus retain the memory of the initial destabilization and their disturbance is what maintains the growth in sectors in the long term. However, most of the destabilizations that will occur later will fail to create radial splits. Instead they will generate fjords of different length with a shape given by advection on the mean profile of the finger in the initial wedge. In turn these structures will destabilize and form new fjords. The problem is then that most of the third-order or fourth-order wedges become more and more distorted compared to the known straight wedges so that the fits become less convincing.

In the confined cases it is interesting to note that the instability of the tip is able to generate the structures of all sizes needed for the build-up of the fractal structure. In reverse it has the same limits. For instance, in linear cells it is well known that the fractal range of scales is bound by l_c and W; the tip instability produces branches similarly bound. This can be understood as follows: the screening off is responsible for the upper bound on the size of the secondary structures. This screening off is also responsible for the stable finger shape.

There is an interesting correspondence between the present work and recent theoretical approaches to unsteady patterns by Tanveer (1991), Elezgaray (1998) and Kessler *et al.* (1998). In their work they use conformal transform techniques and show that the formation of successive fjords in the real cell correspond to singularities of the complex plane moving from infinity towards the unit circle. It would be interesting to see whether or not their approach could lead to a generalization of our results.

We can note that it should also be possible to extend this type of analysis to other situations. For instance in the directional growth of crystals there is a regime often called the seaweed morphology (Ihle & Müller-Krumbhaar 1994). In this type of growth (which occurs in isotropic conditions when the imposed gradient is weak) large cells are formed, each of them being unstable and having imperfect splitting. The shape of the observed fjords appears to be curves normal to the cells profiles. This is also observed in the growth of eutectics (Akamatsu & Faivre 1999). Similarly, during the growth of sponges and stony corals there are steady regimes forming column-shaped colonies (see Kaandorp 1993 and references therein). The individual coralites appear oriented along the normal curves to the outer profile. The normal profiles are then clearly visible on cross-sections of these structures.

We thank Martine Ben Amar, Juan Elezgaray and Stéphane Douady for helpful discussions and the first of these for providing us with the numerical profiles of stable fingers in a variety of sector-shaped cells. We are grateful to Eric Janiaud for his contribution to the experimental work. E. Lajeunesse thanks DGA/DSP for making possible his stay at LPS.

REFERENCES

Akamatsu, S. & Faivre, G. 2000 Travelling waves, two phase fingers and eutectic colonies in thin-sample directional solidification of a ternary eutectic alloy. *Phys Rev.* E **61**, 3757–3770.

Aldushin, A. P. & Matkowsky, M. 1999 Extremum principles for selection in the Saffman–Taylor finger and Taylor–Saffman bubble problem. *Phys. Fluids* **11**, 1287–1296.

Argoul, F., Arnéodo, A., Elezgaray, J., Grasseau, G. & Murenzi, R. 1990 Wavelet analysis of the self-similarity of diffusion limited aggregates and electrodeposition clusters. *Phys Rev.* A **41**, 5537–5560.

Arnéodo, A., Couder, Y., Grasseau, G., Hakim, V. & Rabaud, M. 1989 Uncovering the analytical Saffman–Taylor finger in unstable viscous fingering and diffusion limited aggregation. *Phys. Rev. Lett.* **63**, 984–987.

Arnéodo, A., Elezgaray, J., Tabard, M. & Tallet, F. 1996 Statistical analysis of off-lattice diffusion limited aggregates in channel and sector geometries. *Phys Rev.* E **53**, 6200–6223.

Bataille, J. 1968 Stabilité d'un écoulement radial non miscible. *Revue Inst. Pétrole* **23**, 1349–1364.

Ben Amar, M. 1991 Exact self-similar shapes in viscous fingering. *Phys. Rev.* A **43**, 5724–5727.

Ben Amar, M., Hakim, V., Mashaal, M. & Couder, Y. 1991 Self dilating fingers in wedge shaped Hele-Shaw cells. *Phys. Fluids* A **3**, 1687–1690.

Bensimon, D. 1986 On the stability of viscous fingering. *Phys. Rev.* A **33**, 1302–1308.

Bensimon, D., Pelcé, P. & Shraiman, B. I. 1987 Dynamics of curved fronts and pattern selection. *J. Phys. Paris* **48**, 2081–2087.

Brenner, E., Levine, H. & Tu, Y. 1991 Mean field theory for the diffusion-limited aggregation in low dimensions. *Phys. Rev. Lett.* **66**, 1978–1981.

Caroli, B., Caroli, C. & Roulet, B. 1987 On the linear stability of needle crystals: evolution of a Zel'dovich localised front deformation. *J. Phys. Paris* **48**, 1423–1437.

Chuoke, R. L., Van Meurs, P. & Van der Pol, C. 1959 The instability of slow immiscible viscous liquid–liquid displacements in permeable media. *Petrol. Trans. AIME* **216**, 188–194.

Combescot, R. & Ben Amar M. 1991 Selection of Saffman–Taylor fingers in the sector geometry. *Phys. Rev. Lett.* **67**, 453–456.

Combescot, R., Dombre, T., Hakim, V. & Pomeau, Y. 1986 Shape selection of the Saffman–Taylor fingers. *Phys. Rev. Lett.* **56**, 2036–2039.

Combescot, R., Dombre, T., Hakim, V., Pomeau, Y. & Pumir, A. 1988 Analytic theory of the Saffman–Taylor fingers. *Phys. Rev.* A **37**, 1270–1283.

Couder, Y. 1988 Viscous fingering in a circular geometry. In *Random Fluctuations and Pattern Growth* (ed. H. E. Stanley & N. Ostrowsky), pp. 75–81. Kluwer.

Couder, Y. 1991 Growth patterns: from the stable curved fronts to fractal structures. In *Chaos, Order and Patterns* (ed. R. Artuso, P. Cvitanovic & G. Casati), pp. 203–227. Plenum.

De Gregoria, A. J. & Schwartz, L. W. 1986 A boundary integral method for two phases displacements in Hele-Shaw cells. *J. Fluid Mech.* **164**, 383–400.

Elezgaray, J. 1998 Modelling the singularity dynamics of a Hele-Shaw flow. *Phys. Rev.* E **57**, 6884–6887.

Hong, D. C. & Langer, J. S. 1986 Analytical theory of the selection mechanism in the Saffman–Taylor problem. *Phys. Rev. Lett.* **56**, 2032–2035.

Howison, S. D. 1986 Fingering in Hele-Shaw cells. *J. Fluid Mech.* **167**, 439–453.

Ihle, T. & Müller-Krumbhaar, H. 1994 Fractal and compact growth morphologies in phase transitions with diffusion transport. *Phys. Rev.* E **49**, 2972–2991.

Kaandorp, J. A. 1993 Simulating radiate accretive growth using iterative geometric constructions. In *Growth Patterns in Physical sciences and Biology* (ed. Garcia Luiz, E. Louis, P. Meakin & L. M. Sander). Plenum.

Kessler, D., Koplik, J. & Levine, H. 1988 Pattern selection in fingered growth phenomena. *Adv. Phys.* **37**, 255–339.

Kessler, D. A., Olami, Z., Oz, J., Procaccia, I., Somfai, E. & Sander, L. M. 1998 Diffusion limited aggregation and viscous fingering in a wedge: evidence for a critical angle. *Phys. Rev.* E **57**, 6913–6916.

Kopf-Sill, A. R. & Homsy, G. M. 1988 Nonlinear unstable viscous fingers in Hele-Shaw flows, I. Experiments. *Phys. Fluids* **31**, 242–249.

Levine, H. & Tu, Y. 1992 Mean field diffusion limited aggregation in radial geometries. *Phys. Rev.* A **45**, 1053–1057.

McLean, J. W. & Saffman, P. G. 1981 The effect of surface tension on the shape of fingers in a Hele-Shaw cell. *J. Fluid Mech.* **102**, 455–469.

May, S. E. & Maher, J. V. 1989 Fractal dimension of radial fingering patterns. *Phys. Rev.* A **40**, 1723–1726.

Mineev-Weinstein, M. 1998 Selection of the Saffman–Taylor finger width in the absence of surface tension, an exact result. *Phys. Rev. Lett.* **80**, 2113–2116.

Park, C. W. & Homsy, G. M. 1985 The instability of long fingers in Hele-Shaw flows. *Phys. Fluids* **28**, 1583–1585.

Paterson, L. 1981 Radial viscous fingering in a Hele-Shaw cell, *J. Fluid Mech.* **113**, 513–529.

Paterson, L. 1984 Diffusion limited aggregation and two fluid displacements in porous media. *Phys. Rev. Lett.* **52**, 1621–1623.

Pelcé, P. 1988 *Dynamics of Curved Fronts.* Academic.

Rabaud, M., Couder, Y. & Gerard, N. 1988 The dynamics and stability of anomalous Saffman–Taylor fingers. *Phys. Rev.* A **37**, 935–947.

Rauseo, S. N., Barnes, P. D. & Maher, J. V. 1987 Development of radial fingering patterns. *Phys. Rev.* A **35**, 1245–1251.

Saffman, P. G. & Taylor, G. I. 1958 The penetration of a fluid into a porous medium or Hele-Shaw cell containing a more viscous fluid. *Proc. R. Soc. Lond.* A **245**, 312–329.

Shraiman, B. 1986 Velocity selection in the Saffman–Taylor problem. *Phys. Rev. Lett.* **56**, 2028–2031.

Tabeling, P., Zocchi, G. & Libchaber, A. 1987 An experimental study of the Saffman–Taylor instability. *J. Fluid Mech.* **177**, 67–82.

Tanveer, S. 1987 Analytic theory of the linear stability of the Saffman–Taylor finger. *Phys. Fluids* **30**, 2318–2329.

Tanveer, S. 1991 Viscous displacement in a Hele-Shaw cell. In *Asymptotics Beyond all Orders* (ed. H. Segur, S. Tanveer & H. Levine), p. 131. Plenum.

Thomé, H., Rabaud, M., Hakim, V. & Couder, Y. 1989 The Saffman–Taylor instability: from the linear to the circular geometry. *Phys. Fluids* A **1**, 224–240.

Vanden-Broeck, J. M. 1983 Fingers in a Hele-Shaw cell with surface tension. *Phys. Fluids* **26**, 2033–2034.

Witten, T. & Sander, L. M. 1981 Diffusion limited aggregation, a kinetic critical phenomenon. *Phys. Rev. Lett.* **47**, 1400–1403.

Witten, T. & Sander, L. M. 1983 Diffusion-limited aggregation. *Phys. Rev.* B **27**, 5686–5697.

Zel'dovich, Ya. B., Istratov, A. G., Kidin, N. I. & Librovich, V. B. 1980 Flame propagation in tubes: hydrodynamics and stability. *Combust. Sci. Technol.* **24**, 1–13.